The Influence of Lateral Advection on the Residual Estuarine Circulation: A Numerical Modeling Study of the Hudson River Estuary

MALCOLM E. SCULLY

Center for Coastal Physical Oceanography, Old Dominion University, Norfolk, Virginia

W. ROCKWELL GEYER

Applied Ocean Physics and Engineering, Woods Hole Oceanographic Institution, Woods Hole, Massachusetts

JAMES A. LERCZAK

College of Oceanic and Atmospheric Sciences, Oregon State University, Corvallis, Oregon

(Manuscript received 20 November 2007, in final form 3 July 2008)

ABSTRACT

In most estuarine systems it is assumed that the dominant along-channel momentum balance is between the integrated pressure gradient and bed stress. Scaling the amplitude of the estuarine circulation based on this balance has been shown to have predictive skill. However, a number of authors recently highlighted important nonlinear processes that contribute to the subtidal dynamics at leading order. In this study, a previously validated numerical model of the Hudson River estuary is used to examine the forces driving the residual estuarine circulation and to test the predictive skill of two linear scaling relationships. Results demonstrate that the nonlinear advective acceleration terms contribute to the subtidal along-channel momentum balance at leading order. The contribution of these nonlinear terms is driven largely by secondary lateral flows. Under a range of forcing conditions in the model runs, the advective acceleration terms nearly always act in concert with the baroclinic pressure gradient, reinforcing the residual circulation. Despite the strong contribution of the nonlinear advective terms to the subtidal dynamical balance, a linear scaling accurately predicts the strength of the observed residual circulation in the model. However, this result is largely fortuitous, as this scaling does not account for two processes that are fundamental to the estuarine circulation. The skill of this scaling results because of the compensatory relationship between the contribution of the advective acceleration terms and the suppression of turbulence due to density stratification. Both of these processes, neither of which is accounted for in the linear scaling, increase the residual estuarine circulation but have an opposite dependence on tidal amplitude and, consequently, strength of stratification.

I. Introduction

The first dynamic theory for the processes that drive the tidally averaged residual circulation in estuaries was developed by Pritchard (1952, 1954, 1956) in his pioneering study of the James River. His work describing the balance between the seaward-directed barotropic pressure gradient, the landward-directed baroclinic pressure gradient, and the stress divergence associated with residual velocity shear has served as the foundation for the understanding of estuarine dynamics for over 50 years. Both Hansen and Rattray (1965) and Chatwin (1976) use this balance to predict the amplitude of the residual circulation. In many applications, the stress is parameterized in terms of a vertically and tidally averaged eddy viscosity acting on the tidally averaged vertical velocity shear. Using physically realistic values for the eddy coefficient, this approach has predicted the strength of the residual circulation in a number of estuaries, including the Hudson River, with skill (Geyer et al. 2000; MacCready 2007; Ralston et al. 2008).

One difficulty in the application of this scaling is determining the appropriate parameterization of eddy vis-

Corresponding author address: Malcolm E. Scully, 4111 Monarch Way, Norfolk, VA 23508.
E-mail: mscully@odu.edu

DOI: 10.1175/2008JPO3952.1

cosity and its dependence on internal variables, such as stratification, and external variables, such as freshwater discharge and tidal amplitude. It is widely acknowledged that vertical density stratification significantly impacts the internal friction and, as a consequence, the strength of the residual estuarine circulation is sensitive to the stability of the water column (Uncles and Stephens 1990; Monismith et al. 2002; Scully et al. 2005). The impact of density stratification on vertical mixing in estuaries has been documented by direct field measurements of turbulent fluxes (Stacey et al. 1999; Scully and Friedrichs 2003, 2007). However, previous studies of the residual circulation in the Hudson River do not demonstrate a strong sensitivity to stratification. Geyer et al. (2000) used measurements of the tidal variations in the vertically integrated acceleration and pressure gradient terms to obtain vertical profiles of stress. Based on these estimates, they concluded that the tidally averaged interfacial stress between the inflowing and outflowing layers was negligible and that the strength of the residual velocity depended only on the intensity of the bottom mixing and the along-channel density gradient. This result suggests that, in an estuary with large spring–neap variations in stratification, the strength of the residual circulation would be relatively insensitive to the influence of stratification on the turbulent momentum flux across the exchange interface. Geyer et al. presented a model in which the bottom mixing was parameterized using the amplitude of the tidal flow and a drag coefficient and were able to accurately predict the strength of the residual estuarine circulation in the Hudson River. MacCready (2007) proposed an analytical model that extends the results of Hansen and Rattray (1965) to consider time dependence and variable bathymetry, which utilizes the Geyer et al. scaling to parameterize the tidally averaged eddy viscosity. MacCready's results compare favorably with observations from the Hudson River and San Francisco Bay, but did not agree well with observations from Delaware Bay. More recently, this model was used by Ralston et al. (2008) and shows skill when compared with an extensive dataset describing the residual estuarine circulation and subtidal salinity structure of the Hudson River.

While the parameterization of the vertical turbulent salt and momentum flux in these models is appealing, a significant shortcoming may be the omission of the redistribution of momentum by lateral circulations. Trowbridge et al. (1999) found significant differences between direct measurements of bed stress and the integral of the simplified momentum balance suggested by Geyer et al., particularly during spring tides. They suggested that advective nonlinearities might explain the discrepancies. The role of lateral advection was more clearly illustrated in the idealized estuarine simulations of Lerczak and Geyer (2004). Their results show that advection by lateral flows acts as a driving force for the residual estuarine circulation and can be larger than the along-channel pressure gradient under weakly stratified conditions. As result, the strength of the residual estuarine circulation predicted by their model was stronger during spring tides than predicted by the Hansen and Rattray (1965) scaling and, thus, had a smaller than expected dependence on the eddy viscosity.

The results of Lerczak and Geyer (2004) challenge the notion that the strength of the residual estuarine circulation can be simply parameterized using existing linear scalings. The goal of this paper is to explore the mechanisms driving the subtidal residual estuarine circulation in the Hudson River estuary utilizing a previously validated numerical model (Warner et al. 2005). This paper will build on the results of Lerczak and Geyer by using realistic bathymetry and forcing, as well as a two-equation turbulence closure scheme. The primary focus will be to explore the apparent paradox presented by the results of Lerczak and Geyer (2004) and Geyer et al. (2000): If the nonlinear advective terms contribute to the subtidal along-channel momentum balance at leading order, why does a linear scaling that represents the residual estuarine circulation as the balance between a baroclinic pressure gradient and bottom friction show predictive skill? In section 2, the numerical and analytical methods utilized are explained. The model results are presented in section 3, including the dominant terms in the subtidal along-channel momentum balance and description of the lateral dynamics. The results from the numerical model are compared with the analytic representations of the residual estuarine circulation and discussed in section 4, and conclusions are presented in section 5.

2. Methods

a. Numerical model

The numerical simulations in this study were conducted utilizing the Regional Ocean Modeling System (ROMS). The model was implemented in a manner consistent with the previously published results of Warner et al. (2005). The model domain is identical to that used by Warner et al. and consists of $200 \times 20 \times 20$ curvilinear grid that spans the 250 km from the Battery to the Federal Dam in Troy, New York (Fig. 1). In the lower reaches of the estuary, the grid spacing is approximately 300 m in the along-channel direction and 100 m in the across-channel direction. The along-

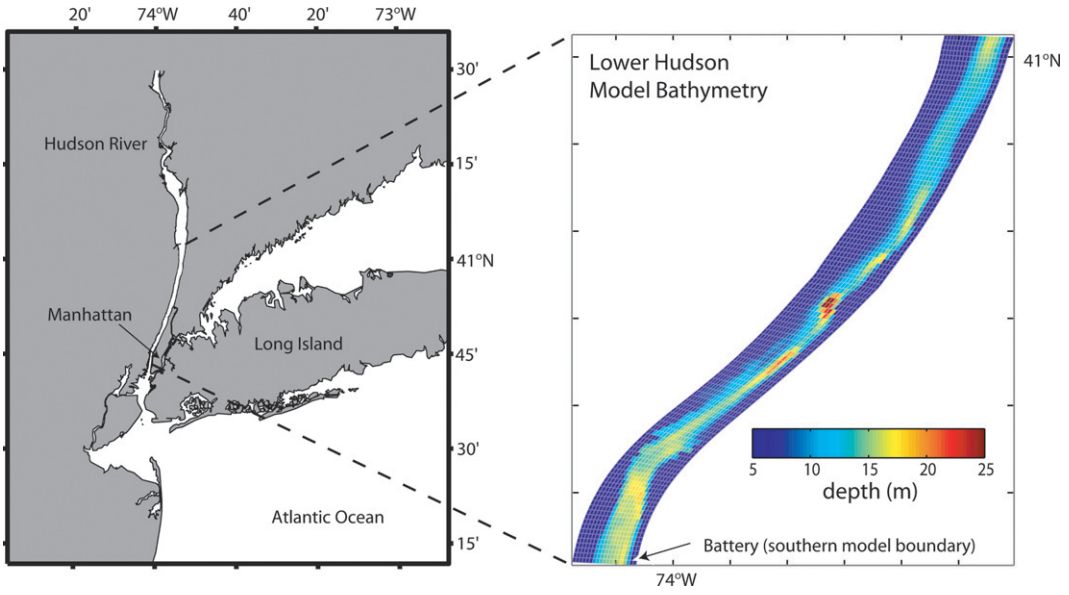

FIG. 1. Study site with lower reaches of numerical model domain. See Warner et al. (2005) for complete grid.

channel grid spacing increases linearly in the region 40 to 250 km north of the Battery. There are 20 terrain-following sigma layers in the vertical dimension. While Warner et al. used observed time series of sea level elevation at the Battery to force the model at the southern boundary, we apply a more idealized implementation by specifying only the M_2 and S_2 tidal constituents. This forcing results in a spring–neap modulation of the salinity stratification that varies in a manner consistent with both the model results of Warner et al. (2005) as well as previously published data (Lerczak et al. 2006). Salinity at the southern boundary was specified following the gradient formulation proposed by Warner et al., which specifies a salinity gradient as a function of river discharge. A fixed temperature of 10°C was imposed on both boundaries and held constant throughout the domain. The model was run for four values of river discharge: 150, 300, 600, and 1200 $m^3\ s^{-1}$ consistent with the typical seasonal variability. River discharge was prescribed by imposing a tidally and cross-sectionally averaged southerly directed mean flow at both northern and southern boundaries. Salinity of the inflow at the northern boundary was set to zero. The generic length-scale turbulence closure parameterization was used with the stability functions of Kantha and Clayson (1994). Warner et al. (2005) demonstrated that the model results for the Hudson River were largely insensitive the choice of turbulence closure. Following Warner et al., the background vertical viscosity and diffusivity were set equal to $5 \times 10^{-6}\ m^2\ s^{-1}$. The surface stress was set to zero and the bottom momentum boundary condition was imposed by assuming a logarithmic velocity for the bottom grid cell using a roughness length of 0.002 m. A no-slip condition was applied at the lateral boundaries. The model was initiated from rest utilizing an idealized along-channel salinity distribution and the model was run until the salinity field equilibrated with the forcing, which occurred after approximately 10 days. The model was then restarted and run for 45 days to capture the full spring–neap variability.

b. Momentum balance

One of the goals of this paper is to quantify the dominant along-channel forcing driving the residual estuarine circulation. At subtidal time scales the along-channel momentum balance can be represented as

$$\frac{1}{\rho_o}\left\langle\frac{\partial P}{\partial x}\right\rangle + \left\langle u\frac{\partial u}{\partial x}\right\rangle + \left\langle v\frac{\partial u}{\partial y}\right\rangle + \left\langle w\frac{\partial u}{\partial z}\right\rangle = -\frac{1}{\rho_o}\left\langle\frac{\partial \tau}{\partial z}\right\rangle. \quad (1)$$

The first term is the pressure gradient and consists of both a baroclinic and barotropic component. The remaining terms on the left-hand side of the equation represent the nonlinear advective terms; the stress divergence is on the right-hand side; and the angle brackets denote tidally averaged quantities. At subtidal time scales, the balance is approximately steady with little contribution from the tendency term ($\partial u/\partial t$) or the Coriolis acceleration (fv), which have been omitted from (1).

To simplify the analysis in several sections of this paper, a layer-averaged approach will be used. The fact

that, generally, there is a landward-directed residual circulation near the bed and a seaward-directed residual higher in the water column provides a natural framework for this approach. At each cross section in the estuarine portion of the model domain, the tidally averaged along-channel transport is calculated. An inflowing layer is defined where the residual transport is directed landward and, conversely, an outflowing layer is defined where the subtidal flux is seaward. The residual estuarine circulation (U_E) is defined as the subtidal velocity of the lower layer, which is calculated by dividing the flux of water into the estuary by the cross-sectional area of the lower layer through which it is flowing. Top-to-bottom salinity stratification (ΔS) is reported as the difference between the layer-averaged quantities.

To examine the forces that are driving the residual estuarine circulation over the entire estuarine portion of the model domain, we integrate the terms in Eq. (1) over the volume of the inflowing lower layer, normalizing each term by the interfacial surface area (A) between the residual inflowing and outflowing layers. The resulting layer-integrated quantities have units of momentum flux ($m^2\ s^{-2}$). For example, the layer-integrated pressure gradient term for the bottom layer is defined as

$$\frac{1}{\rho_o}\overline{\int\left\langle\frac{\partial P}{\partial x}\partial z\right\rangle}\equiv\frac{1}{\rho_o}\frac{1}{A}\int_L^0\int_{w_2(z)}^{w_1(z)}\int_{-H(y)}^{-h_1(y)}\left\langle\frac{\partial P}{\partial x}\partial z\right\rangle\partial y\partial x, \tag{2}$$

where h_1 is the depth of the interface between the inflowing and outflowing layers, H is the total water depth, w_1 and w_2 are the lateral boundaries of the bottom layer, L is the length of the salt intrusion, and the angle bracket indicates a tidally averaged quantity. The overbar in (2) denotes that the quantities have been averaged spatially over the estuarine portion of the model domain. Using this notation, the dominant subtidal momentum balance for the inflowing layer can be written as

$$\frac{1}{\rho_o}\overline{\int\left\langle\frac{\partial P}{\partial x}\partial z\right\rangle}+\overline{\int\left\langle v\frac{\partial u}{\partial y}\partial z\right\rangle}+\overline{\int\left\langle w\frac{\partial u}{\partial z}\partial z\right\rangle}=-\frac{1}{\rho_o}\left[\overline{\langle\tau_b\rangle}-\overline{\langle\tau_i\rangle}\right]. \tag{3}$$

Here the first term represents the momentum imparted on the flow by the pressure gradient. The second and third terms on the lhs of (3) represent the advective momentum flux between the upper and lower layers by lateral circulation. The first term inside the brackets of the rhs of (3) is the bed stress representing the loss of momentum by the lower layer to bottom friction, and the second term is the interfacial stress representing the turbulent flux of momentum between the two layers. For all of the model runs considered, the Coriolis forcing is negligible and is not considered in the subtidal along-channel dynamics (although its influence on the lateral circulation is significant, as will be discussed below). Previous numerical studies (Lerczak and Geyer, 2004), as well as simple scaling relationships, demonstrate that the along-channel advective acceleration ($u\partial u/\partial x$) is an order of magnitude smaller than the lateral advective terms ($v\partial u/\partial y$ and $w\partial u/\partial z$), which are considered together in this analysis.

c. *Linear scaling of the residual estuarine circulation*

Another important goal of this paper is to examine the skill of linear relationships in predicting the strength of the residual estuarine circulation. The traditional scaling for strength of the subtidal estuarine circulation, as proposed by Hansen and Rattray (1965), is

$$U_E=\frac{g}{C_o\rho_o}\frac{\partial\rho}{\partial x}\frac{H^3}{A_z}, \tag{4}$$

where g is the gravitational acceleration, ρ_o is the background density, $\partial\rho/\partial x$ is the along- channel density gradient, H is the water depth, A_z is the tidally averaged vertical eddy viscosity, and C_o is an integration constant. If it is assumed that the channel depth does not vary laterally and that A_z does not vary with depth, the value of C_o is 48. By utilizing a numerical model, all of the quantities in (4) are easily obtained, so it is straightforward to compare the strength of the residual estuarine circulation predicted by the model to that predicted by the Hansen and Rattray scaling. Because the cross-sectional depth is not constant and the tidally averaged eddy viscosity is not constant in the vertical or lateral dimension, the value of the C_o is not known. We therefore estimate the value of this coefficient based on the best fit between the numerical prediction and this scaling. In applying this scaling, we use the cross-sectionally averaged depth for H. The eddy viscosity is averaged over the cross section and then low-pass filtered with a 35-h cutoff to remove tidal variations. The along-channel density gradient is calculated in a similar way. The value of C_o is calculated from a least squares linear regression between U_E and the remaining terms on the lhs of Eq. (4), forced through the origin.

Building on the work of Godfrey (1980), Geyer et al. (2000) provided an alternative scaling that does not rely on a poorly constrained eddy coefficient. They pro-

posed a two-layer model in which the dominant along-channel balance in the lower layer was between the baroclinic forcing and the bottom stress. Assuming that the inflowing and outflowing layers are roughly the same thickness, their scaling for the strength of the residual estuarine circulation can be written as

$$U_E = \frac{1}{A_o}\frac{g}{\rho_o}\frac{\partial \rho}{\partial x}\frac{H^2}{U_t C_D} = \frac{u_t \mathrm{Ri}_x}{A_o}, \quad (5)$$

where C_D is a drag coefficient (~0.0025), U_t is the amplitude of the near-bottom along-channel tidal currents, and A_o is a constant. This scaling can be represented by the horizontal Richardson number (Ri_x), which can be thought of as a ratio of the baroclinic forcing to the bed stress (Stacey et al. 2001). As with the value of C_o, discussed above, the value of A_o will be treated as an empirical coefficient, fit to the results of the numerical simulations.

3. Results

a. Subtidal residual estuarine circulation and stratification

We begin by describing the model results for low discharge conditions (150 $m^3\ s^{-1}$). We will focus on a midestuary location (~23 km north of the Battery) that has been the focus of several field studies in the Hudson River (Geyer et al. 2000; Lerczak et al. 2006). Figure 2 shows contours of the residual velocity and salinity fields, as well as the subtidal variations of the residual estuarine circulation, the salinity stratification, the along-channel density gradient, and the cross-sectionally averaged eddy viscosity predicted by the model for this location. There is a clear spring–neap modulation of both the residual estuarine circulation and vertical density stratification. During the less energetic neap conditions, the residual estuarine circulation is enhanced, with the residual velocity exceeding 10 cm s^{-1}. During spring tidal conditions, the residual estuarine circulation is weaker with residual velocities of approximately 40% of their value during neap conditions. Salinity stratification exhibits a pattern consistent with the residual estuarine circulation, with greater stratification occurring during neap conditions, when the creation of stratification by along-channel advection is strong and the destruction of stratification by turbulent mixing is weak. Spring–neap variations in the along-channel density gradient are weak, and the modulation of residual estuarine circulation and stratification appears to be mainly related to the spring–neap variations in mixing. There is some along-estuary variability, but the patterns depicted in Fig. 2 are largely representative of both the strength and subtidal phasing of the residual estuarine circulation and stratification along the system.

b. Subtidal along-channel momentum balance

We can evaluate the forces driving the circulation in detail by examining the dominant terms in the subtidal along-channel momentum balance. Figure 3 shows contours of the dominant terms in the momentum balance for spring and neap tidal conditions. At subtidal time scales, the Coriolis and acceleration terms are negligible and the dominant balance is between the pressure gradient, stress divergence, and advective acceleration terms. Consistent with the results of Lerczak and Geyer (2004), during both spring and neap tidal conditions the magnitude of the advective acceleration terms is comparable to the magnitude of the residual pressure gradient (also see Table 1). During spring and neap tidal conditions, maximum values for the subtidal pressure gradient and advective acceleration terms both approach 3×10^{-5} m s^{-2}. Values of the stress divergence approach 6×10^{-5} m s^{-2}, balancing the combined forcing of the pressure gradient and advective terms.

While the spatial distribution of the subtidal advective terms is somewhat complex, several important patterns emerge. During spring tides the advective acceleration largely augments the residual pressure gradient. The advective acceleration terms are, on average, directed landward over the deeper channel areas and seaward over the shallower shoals. As a result, they are a significant driving force for the residual estuarine circulation during spring tidal conditions. During neap tidal conditions the spatial distribution of the subtidal advective acceleration terms is more complex (Fig. 3e). Over the channel the subtidal contribution of the advective terms augments the landward-directed net pressure forcing near the bed. However, because of the three-layer structure of the advective terms, they oppose the pressure forcing over significant areas of the cross section. Despite their more complex spatial structure during neap tidal conditions, the overall contribution of the advective terms is directed landward over the channel and seaward over the shoals, in a depth-averaged sense.

The role of the advective terms in driving the residual estuarine circulation can be illustrated more clearly by examining the integrated forces acting on the bottom inflowing layer. These terms were calculated following the methods outlined in section 2a and then averaged over the entire estuarine portion of the model domain for low river discharge conditions (Fig. 4). Consistent with the results of Lerczak and Geyer (2004), the advective acceleration terms are acting as a driving force

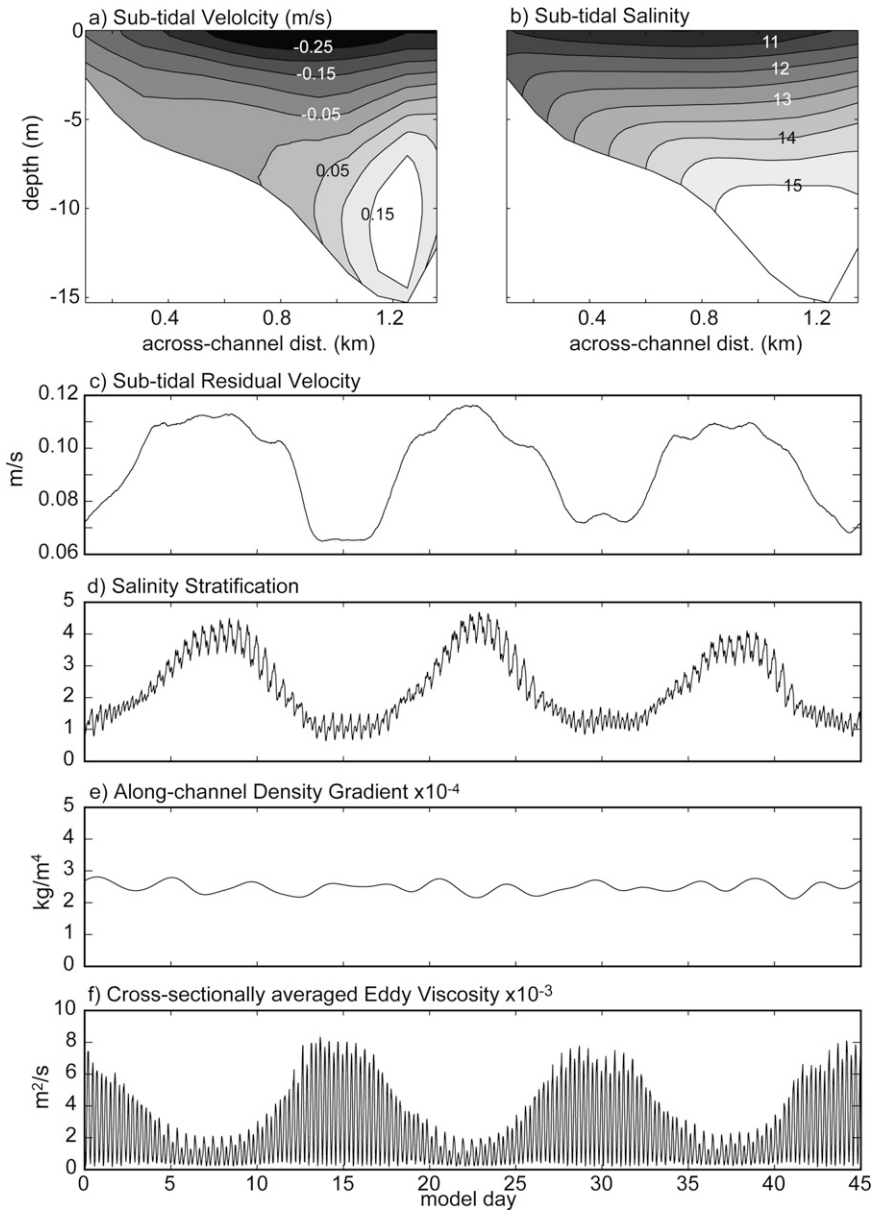

FIG. 2. Model results for cross section, 23 km north of the Battery, for low-discharge conditions (150 m^3 s^{-1}): (a) Subtidal along-channel velocity contours averaged over the spring–neap cycle; (b) subtidal salinity contours averaged over spring–neap cycle; (c) time series of subtidal residual circulation; (d) time series of salinity stratification determined by the difference in average salinity between residually inflowing and outflowing layers; (e) low-pass-filtered longitudinal density gradient; (f) time series of cross-sectionally averaged eddy viscosity.

for the residual estuarine circulation. The advective terms are a source for landward momentum, reinforcing the pressure gradient forcing on the lower layer throughout the spring–neap cycle. The advective forcing is at a maximum during spring tidal conditions, when it approaches 80% of the layer-integrated pressure gradient forcing. The importance of the advective terms is reduced during neap tidal conditions, when it is approximately 40% of the layer-integrated pressure gradient forcing. Both bed stress and interfacial stress act as sinks for landward momentum in the lower layer. There is a strong spring–neap modulation of the tidally averaged interfacial stress, which is largely equal and opposite of the advective momentum flux caused by

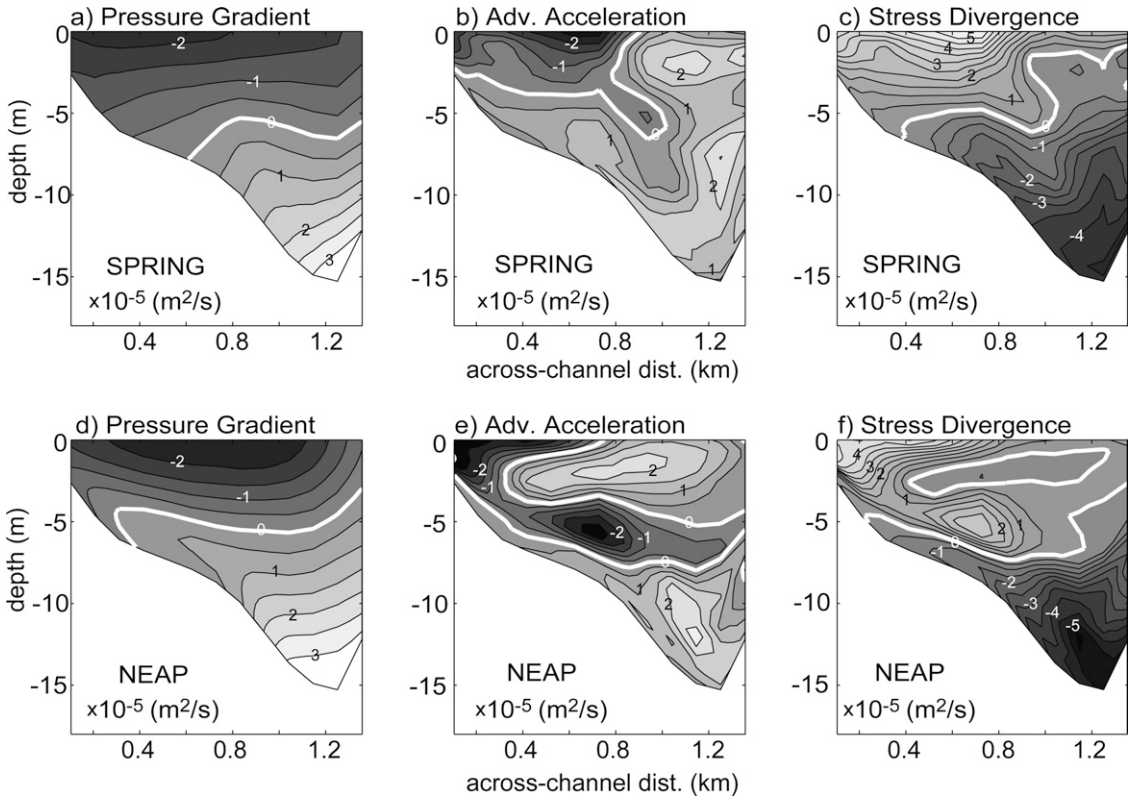

FIG. 3. Contours of the dominant subtidal along-channel momentum terms, for cross section 23 km north of the Battery, for low discharge conditions (150 m^3 s^{-1}): (a) Pressure gradient (spring), (b) $vdu/dy + wdu/dz$ (spring), (c) stress divergence (spring), (d) pressure gradient (neap), (e) $vdu/dy + wdu/dz$ (neap), and (f) stress divergence (neap).

lateral circulation (the implications of this will be discussed in section 4b).

Figure 4 demonstrates that the advective flux of landward momentum into the lower layer acts as a significant driving force for the residual estuarine circulation under low river discharge conditions. The results from the other simulated river discharges are reported in Table 1. In all cases, the tidally averaged advective flux into the lower layer augments the landward-directed pressure forcing. The landward momentum flux acting on the lower layer is balanced by both bed stress and interfacial stress (turbulent momentum flux into the lower layer). Both the tidally averaged pressure gradient forcing and the bed stress increase with increasing river discharge and decreasing tidal energy. In contrast, both advective momentum flux and interfacial stress are reduced with increasing river discharge and decreasing tidal energy. As a result, the relative importance of both the tidally averaged advective and turbulent momentum fluxes to the residual circulation is significantly reduced with increased river discharge and decreased tidal energy.

Integrating the subtidal momentum terms over the lower layer allows a direct comparison of the momentum imparted by the pressure forcing with the momentum flux caused by both advective and turbulent motions. Although this approach highlights the contribution of the dominant terms in the momentum balance at subtidal time scales, it does not reflect the overall magnitude of the terms. In addition to reporting the layer-integrated and tidally averaged momentum terms, Table 1 also reports the total magnitude for the dominant terms in the subtidal momentum balance. The magnitude of the subtidal momentum terms is calculated by integrating the absolute value of the tidally averaged terms in the momentum balance over the entire estuarine cross section. Magnitudes reported in Table 1 are averaged over the entire estuarine portion of the model domain for all simulated river discharges during both spring and neap tidal conditions. In contrast to the tidally averaged advective transfer of momentum into the lower layer, which decreases with increasing river discharge, the overall magnitude of the subtidal advective momentum flux increases substantially with increased river discharge. The magnitude of the subtidal advective momentum flux is always larger

TABLE 1. Comparison of forces driving the residual estuarine circulation (U_E) for numerical model runs with variable river and tidal forcing. All values reported are averaged over the entire estuarine portion of the model domain (where mean salinity >5 psu). Residual velocity (U_E) is calculated by dividing the subtidal flux of water into the estuary by the lower layer area. Salinity stratification (ΔS) is the difference between the residual inflowing and outflowing layers. Lower-layer momentum terms represent the integral of the tidally averaged momentum terms over the residual inflowing lower layer, normalized by the surface area of the interface between the upper and lower layers. Positive values indicate enhancement of landward momentum, while negative values indicate a reduction in landward momentum. The magnitude of the momentum terms is calculated by integrating the absolute value of the tidally averaged value for each term over the entire estuarine domain, normalized by the surface area of the estuary. Values of eddy viscosity represent the tidal average over the entire estuarine portion of the domain. The spatial correlation coefficient is calculated by determining the spatial correlation between the subtidal advective acceleration terms and the baroclinic pressure gradient at every cross section in the estuarine domain and then spatially averaging.

	Spring				Neap			
	Q ($m^3 s^{-1}$)							
	150	300	600	1200	150	300	600	1200
	U_E ($m s^{-1}$)							
	0.05	0.06	0.08	0.10	0.07	0.09	0.10	0.10
	ΔS							
	1.1	2.1	5.5	8.6	3.3	5.0	9.1	10.6
Lower layer integrated momentum terms ($m^2 s^{-2}$) $\times 10^4$								
Pressure gradient forcing	0.27	0.28	0.31	0.53	0.32	0.32	0.45	0.60
Advective momentum flux	0.21	0.22	0.18	0.10	0.13	0.13	0.11	0.11
Bed stress	−0.35	−0.38	−0.38	−0.54	−0.39	−0.40	−0.53	−0.65
Interfacial stress	−0.14	−0.12	−0.11	−0.10	−0.06	−0.05	−0.03	−0.05
Magnitude of integrated momentum terms ($m^2 s^{-2}$) $\times 10^4$								
Pressure gradient forcing	0.95	1.32	1.60	2.39	0.85	1.22	1.65	2.40
Turbulent momentum flux	0.55	0.69	0.72	0.71	0.39	0.45	0.40	0.43
Advective momentum flux	1.11	1.45	1.65	2.35	0.90	1.22	1.59	2.31
Eddy viscosity ($m^2 s^{-1}$) $\times 10^{-4}$	41	36	32	14	17	16	14	8
Spatial correlation coefficient (adv. accel. vs baroclinic ∇p)	0.49	0.44	0.35	0.17	0.32	0.25	0.08	0.02

than the turbulent momentum flux, exceeding it by over a factor of 5 during high discharge neap conditions. Although the magnitude of the subtidal turbulent momentum flux increases with increasing river discharge, this mainly reflects the increased subtidal shear, as the average eddy viscosity decreases with both increased river discharge and decreased tidal energy (Table 1).

The contrast between the magnitude of the advective flux and its contribution to the residual circulation can be explained by examining the spatial correlation between the subtidal advective terms and the baroclinic pressure gradient. In all cases, the spatial correlation between these two terms is positive (albeit weak in some cases), indicating that these two mechanisms are inducing a similar sense of shear in the subtidal flow through the estuarine cross section (e.g., Figure 3). Correlations decrease during neap tidal conditions, as well as with increasing river flow. As a result, the contribution of the advective flux to the residual circulation decreases with increased river discharge despite the fact that the overall magnitude of the advective flux in-

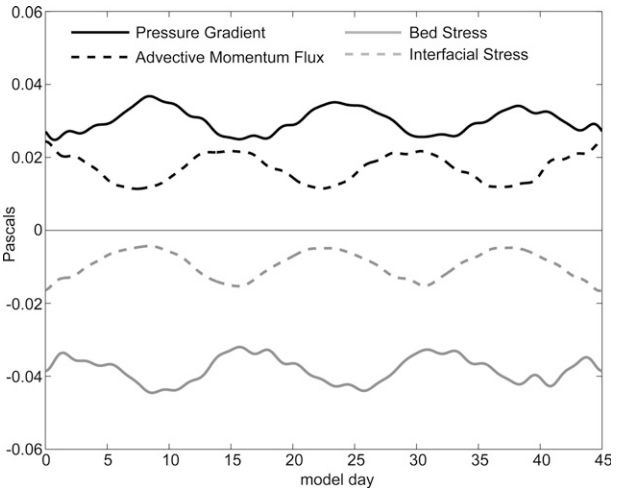

FIG. 4. Time series of the integrated momentum terms acting on the lower (inflowing) layer, averaged over the estuarine portion of the model domain, for low river discharge conditions (150 $m^3 s^{-1}$). The solid black line is the integrated pressure gradient, the dashed black line is the advective momentum flux caused by lateral circulation, the solid gray line is the bed stress, and the dashed gray line is the turbulent momentum flux (interfacial stress).

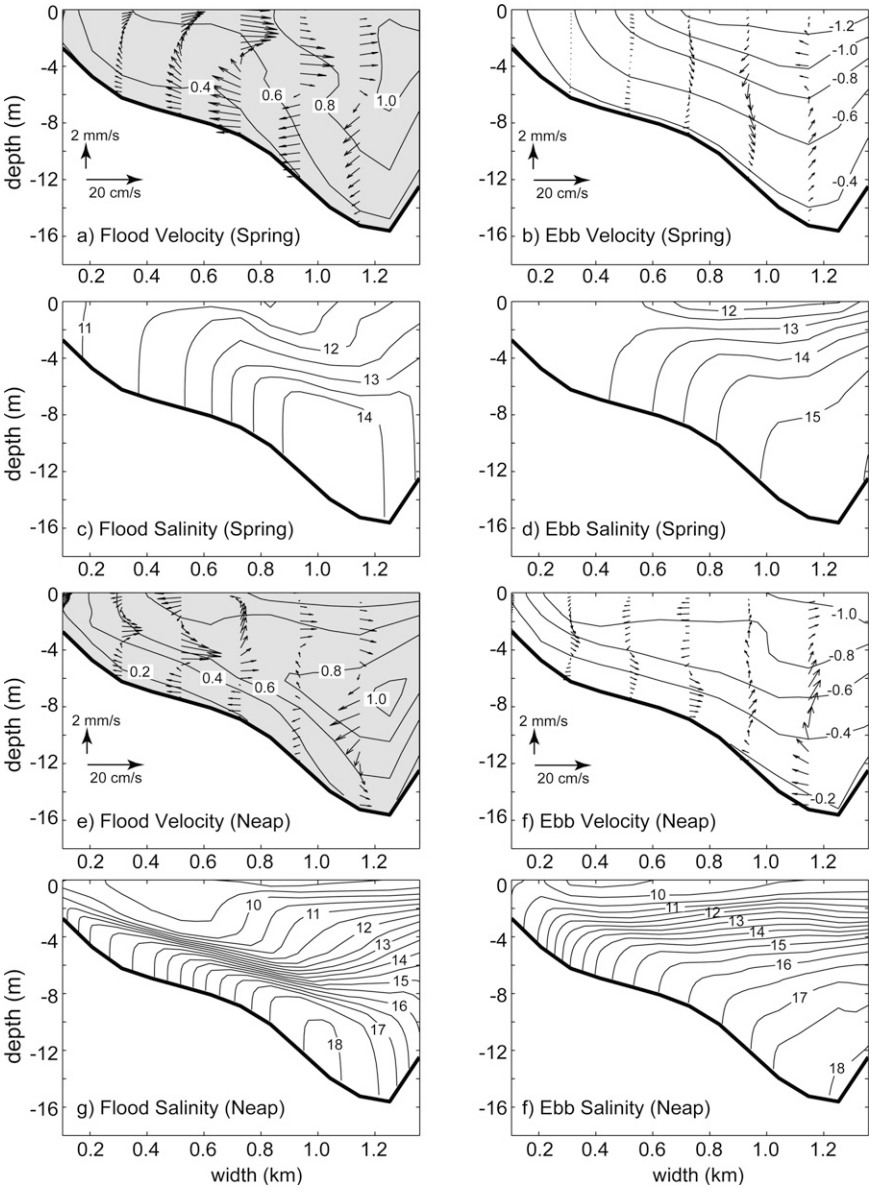

FIG. 5. Contours of velocity and salinity for (a)–(d) spring and (e)–(h) neap conditions, in the cross section 23 km north of the Battery, for low discharge conditions (150 m^3 s^{-1}). Contours are for maximum flood and maximum ebb conditions; along-channel velocity is contoured in 0.20 m s^{-1} intervals and with positive values shaded gray. Lateral flows are shown with arrows, and salinity is contoured in 0.5-psu intervals.

creases significantly. The implications of this will be discussed in more detail in section 4.

c. *Lateral circulation*

The analysis presented above clearly demonstrates that redistribution of momentum by lateral circulation contributes to the subtidal along-channel momentum balance at leading order over a range of conditions. In light of these results, it is instructive to examine the lateral circulation predicted by the model. Figure 5 shows contours of both longitudinal and lateral velocities for peak flood and peak ebb during spring and neap tidal conditions at the estuarine cross section 23 km from the Battery, along with the corresponding salinity contours. During flood tide under spring tidal conditions (Fig. 5a), the lateral velocity exhibits a distinct two-layer structure with the bottom layer flowing toward the left (looking up estuary) and flow toward the

right in the surface layer. The lateral flood velocities during spring tide are relatively strong with maximum values exceeding 10 cm s^{-1}. The two-layer structure in the lateral flow also is apparent during maximum ebb (Fig. 5b); however, the velocities are reduced when compared to flood. The impact of the lateral flow on the salinity structure is apparent in Figs. 5c and 5d. The strong lateral flow during maximum flood induces a significant lateral tilt to the isopycnals, particularly at the top of the bottom boundary layer. During ebb the lateral tilt is reversed, consistent with the thermal wind relationship over much of the cross section.

The two-layer lateral flow during spring tidal conditions is the dominant part of the advective influence on the longitudinal residual estuarine circulation. It significantly impacts both vertical and lateral shear in the residual flow. During flood, the downwelling flow over the deep eastern side of the estuary advects high momentum surface water into the bottom boundary layer, while low momentum boundary layer water from the western shoal is advected toward channel near the surface. This pattern of advection enhances the upestuary momentum near the bed while retarding it near the surface, significantly reducing the vertical shear on flood. Additionally, the downwelling of faster water on the eastern side combined with the upwelling of slower water on the western side induces a lateral shear during flood that favors inflow over the channel (east side).

The general sense of lateral circulation reverses during ebb tide; however, the magnitude of the flow is weaker than observed during flood tide. There is still a vertical momentum transfer between the faster surface waters and slower boundary layer waters that acts to reduce the vertical shear. However, because the lateral flow is weaker, the impact on the vertical shear is reduced during ebb, as compared to flood. The general sense of circulation during ebb consists of upwelling of slow boundary layer water over the east side and downwelling of faster surface water over the west side. This exerts a lateral torque on the along-channel flow that favors outflow over the shallower western side, which reinforces the lateral shear induced during flood. The net effect of these processes is that the advective acceleration terms enhance both vertical and lateral shear of the residual flow.

The patterns are somewhat more complex during neap tidal conditions. While the direction of the lateral flow in the bottom layer is consistent with those observed during spring tidal conditions, the vertical distribution of the lateral flow exhibits a three-layer circulation (Figs. 5e–f). Similar to the spring tidal conditions, there is a tidal asymmetry in the strength of the lateral circulation with larger lateral velocities during the flood tide. The three-layer lateral circulation leads to a more complex spatial pattern in the subtidal advective terms (Fig. 3e). Over the deepest portion of the channel the subtidal contribution of the advective terms is augmenting the landward-directed net pressure forcing. However, near the surface the advective terms are opposing the pressure forcing. Despite the fact that the magnitude of the subtidal advective terms are comparable between spring and neap, the advective terms contribute more to the residual estuarine circulation during spring tidal conditions because the advective terms are more highly correlated in space with the pressure gradient forcing, as discussed in section 3b. This explains the strong spring–neap modulation of the advective momentum flux shown in Fig. 4, despite the similar magnitude shown in Fig. 3.

d. Lateral dynamic balance

Both the lateral velocity and salinity contours shown in Fig. 5 are consistent with Ekman forcing of the lateral dynamics. Scully (2005) showed that at tidal time scales the lateral dynamic balance in the partially mixed York River estuary was geostrophic at first order. This balance can be written as

$$fu = g\frac{\partial \eta}{\partial y} - \frac{g}{\rho_o}\int \frac{\partial \rho}{\partial y}\,\partial z, \tag{6}$$

where the rotational forces on the along-channel tidal flow (fu) are balanced by the lateral barotropic (first term on right) and baroclinic (second term on right) pressure gradients. We can examine the lateral momentum balance using a layer-averaged approach consistent with that described in section 2. For this analysis, all of the lateral momentum terms are averaged over the surface and bottom layers to simplify the analysis. While this is an oversimplification of the details of the lateral dynamics, it is instructive because it provides insight into the mechanisms that drive the flow in each layer, which ultimately governs the advective exchange of momentum between the two layers. A times series of the tidal lateral momentum balance for each layer is presented in Fig. 6 for spring conditions. Even during spring tidal conditions, when frictional effects should be maximal, the lateral balance in the surface layer is largely geostrophic with the Coriolis acceleration of the tidal flow balanced by the lateral barotropic pressure gradient. The ageostrophic forcing in the surface layer is weak, roughly an order of magnitude smaller than the geostrophic terms. In the bottom layer the dominant balance is between the baroclinic and barotropic pressure gradients and rotation. The lateral baroclinic and barotropic pressure gradient are in opposition and

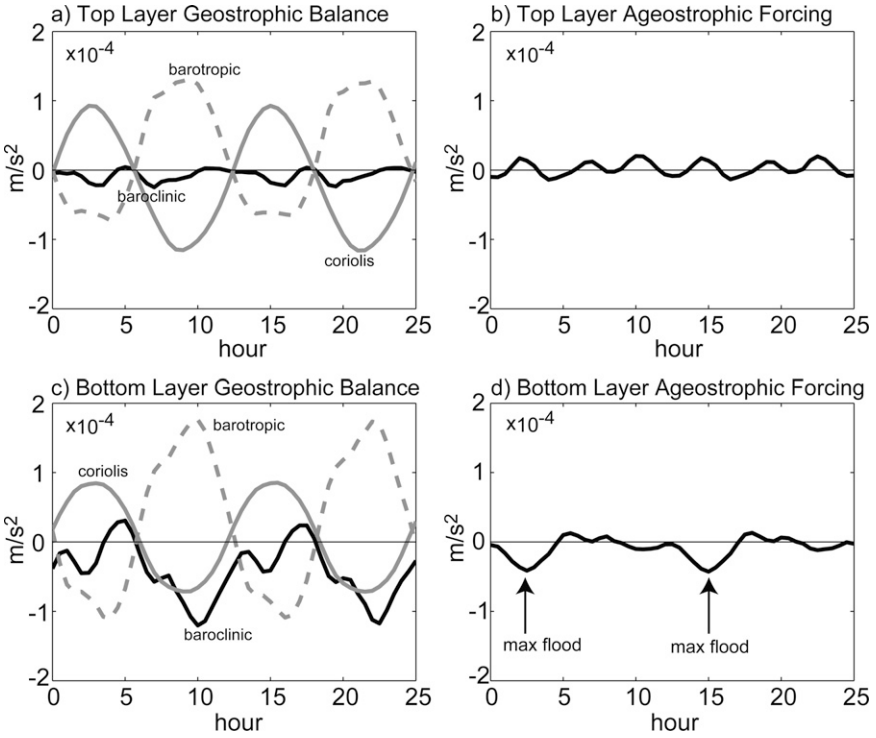

FIG. 6. Tidal lateral momentum balance for spring tidal conditions, in the cross section 23 km north of the Battery, for low discharge conditions (150 $m^3 s^{-1}$). (left) The geostrophic terms: the baroclinic pressure gradient (black line), the barotropic pressure gradient (dashed line), and Coriolis term (gray line). (right) The ageostrophic terms representing the remaining terms in the balance are shown. All terms are averaged over the surface and bottom layers defined subtidally by the zero isopleth. (d) Arrows indicate maximum flooding currents when significant deviations from the geostrophic balance in the lower layer are observed.

nearly 180° out of phase, with the lateral baroclinic pressure gradient responding to the along-channel shear largely via the thermal wind relationship.

The lateral flow in the bottom layer distorts the vertical density stratification, leading to a baroclinic forcing that opposes the bottom Ekman transport. This interaction acts to shut down the lateral Ekman transport in the bottom layer and provides an explanation for the relatively weak lateral flows that occur during ebb tide. In contrast, the geostrophic balance is disrupted during flood, preventing this Ekman shutdown from occurring. While the lateral baroclinic pressure gradient is consistent with the thermal wind relationship during the ebb tide, there is a noticeable deviation several hours into the flood tide. This breaking of the thermal wind allows strong lateral flows to develop during the flood tide (marked with arrows in Fig. 6d). During this period, early in the flood, the ageostrophic terms are maximal, composed mostly of the stress divergence terms. The breaking of the thermal wind balance during the flood tide is consistent with differential advection, which can be caused either by lateral variations in bathymetry or by the lateral shear induced by the lateral advective terms in the along-channel momentum balance (this will be addressed in more detail in section 4c).

4. Discussion

a. Scaling of the residual estuarine circulation

The results from the model demonstrate that the physics driving the residual estuarine circulation is not simply a balance between baroclinic and frictional forcing. The advective acceleration terms contribute to the along-channel momentum balance at leading order, and their contribution cannot be accounted for in the scaling relationships presented in section 2. However, these scalings have been used effectively to predict residual circulation in a number of estuaries, including the Hudson River (Geyer et al. 2000; MacCready 2007). As described in section 2, both the Hansen and Rattray scaling (HR65) and Geyer et al. (2000) scaling (Ri_x) were used to predict the strength of the residual circulation,

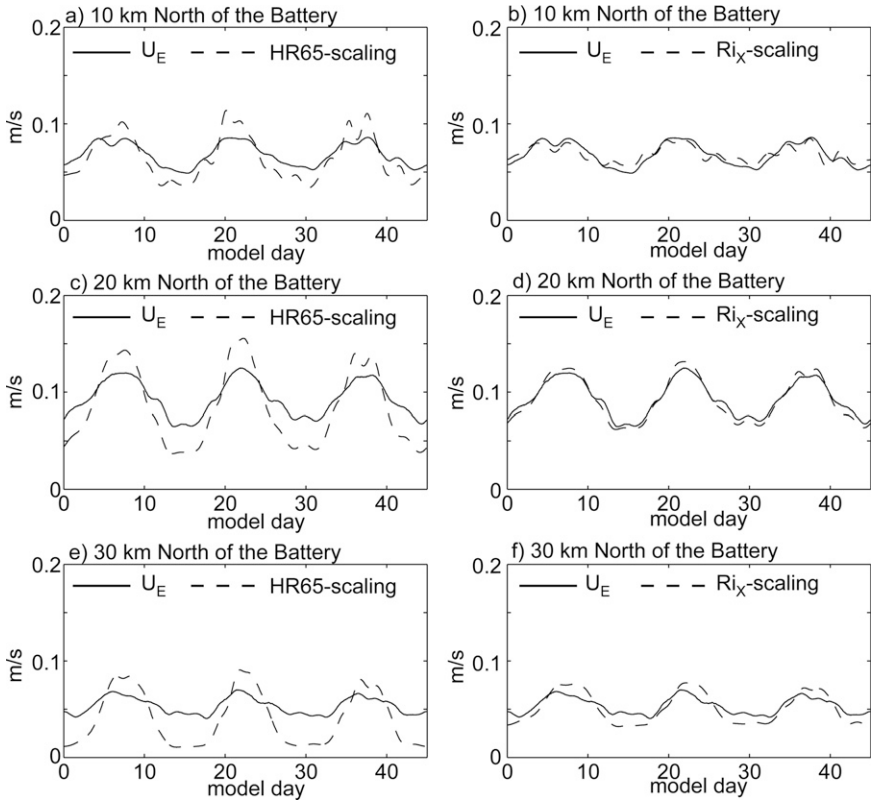

FIG. 7. Comparison of the subtidal residual estuarine circulation predicted by the model (U_E) with the (left) HR65 scaling and (right) Ri_x scaling for evenly spaced locations along the estuary for low river discharge conditions (150 $\mathrm{m^3\ s^{-1}}$). The solid lines present the modeled residual estuarine circulation, and the dashed lines present the predicted residual estuarine circulation from the scaling relationships.

with C_o and A_o used as empirical fitting parameters, which were allowed to vary in space, as well as for various river discharge conditions. Figure 7 shows a comparison of the residual estuarine circulation predicted by both scalings, with the numerical model results from the low-discharge model run. Time series comparisons for several locations at evenly spaced intervals along the estuary are shown. Consistently along the estuary, the HR65 scaling overpredicts the residual estuarine circulation during neap conditions and underpredicts the residual estuarine circulation during spring tidal conditions. While the phasing predicted by the HR65 scaling is roughly consistent with the numerical model results, there is significant error associated with this approach. In comparison, the Ri_x -scaling compares favorably at most locations along the estuary. Table 2 reports the correlation between numerical model results and the prediction of the residual estuarine circulation based on the scaling relationships presented in section 2, as well as the predictive skill as defined by Wilmott (1981):

$$\text{skill} = 1 - \frac{\sum \left| U_{\text{predicted}} - U_{\text{obs}} \right|^2}{\sum \left(\left| U_{\text{predicted}} - \overline{U_{\text{obs}}} \right| + \left| U_{\text{predicted}} - \overline{U_{\text{obs}}} \right| \right)^2}, \tag{7}$$

where $U_{\text{predicted}}$ is the residual estuarine circulation predicted by the scaling and U_{obs} is the residual estuarine circulation from the numerical model. In (7) the overbar indicates time averaging over the entire duration of the data. For all river discharges, the Ri_x scaling is more highly correlated and has higher skill than the HR65 scaling. In all cases, the skill decreases slightly with increasing river discharge.

b. The importance of interfacial stress

The apparent success of the Ri_x scaling is consistent with previously published results for the Hudson River. However, this skill is surprising given that it does not account for a leading-order term in the momentum balance. The greater skill of the Ri_x scaling relative to the

TABLE 2. Comparison of the correlation and skill of two linear scalings of the residual estuarine circulation and their model coefficients. Values for correlation, skill, and the model coefficient (A_o and C_o) are calculated at each cross section within the estuarine portion of the model domain and spatially averaged. Values for the model coefficients are reported for both spring and neap tidal conditions.

	$Q = 150$ m^3 s^{-1}	$Q = 300$ m^3 s^{-1}	$Q = 600$ m^3 s^{-1}	$Q = 1200$ m^3 s^{-1}
	HR65 scaling			
Correlation	0.84	0.84	0.83	0.86
Skill	0.62	0.59	0.60	0.53
C_o (spring)	12.3	16.2	21.1	24.5
C_o (neap)	23.3	28.2	29.6	36.1
	Ri_x scaling			
Correlation	0.92	0.89	0.84	0.92
Skill	0.91	0.88	0.80	0.78
A_o (spring)	2.3	2.4	2.5	2.1
A_o (neap)	2.3	2.4	1.9	1.9

HR65 scaling is particularly surprising because it does not account for the observed dependence of turbulent mixing on stratification. It has been suggested by a number of authors (e.g., Monismith et al. 2002) that increased density stratification significantly damps turbulent mixing, enhancing the strength of the residual estuarine circulation. This effect is accounted for in the application of the HR65 scaling by using the tidally averaged eddy viscosity given by the turbulence closure. However, Fig. 7 suggests that including the influence of stratification on mixing actually reduces the predictive skill of the scaling.

Using the model results, we can examine the impact of density stratification on the turbulent momentum flux between the inflowing and outflowing layers. Figure 8 shows the subtidal variations in salinity stratification and interfacial stress for all four simulated river discharge conditions. In all cases, there is a strong fortnightly modulation of the interfacial stress that is inversely related to the overall salinity stratification. For spring tides during low flow conditions ($Q = 150$ m^3 s^{-1}), the subtidal interfacial stress approaches 0.06 Pa, which is roughly 60% of the value of the bed stress acting on the inflowing layer. In contrast, during neap tidal conditions, the area-averaged interfacial stress is less than 10% of the value of the bed stress. During high flow conditions ($Q = 1200$ m^3 s^{-1}) the spring–neap modulation of the interfacial stress is still apparent; however, the magnitude has been decreased by over 50%, on average. In all cases, the interfacial stress acts to resist the inflowing bottom layer. The strong modulation of the interfacial stress with both changes in tidal energy, as well as river discharge, demonstrates that the presence of density stratification significantly inhibits the exchange of momentum between the inflowing and outflowing layers.

The impact of the interfacial stress is largely accounted for in the HR65 scaling by using the eddy viscosity from the turbulence closure model. However, the significant modulation of the residual estuarine circulation by the advective momentum flux is not accounted for in this approach. As a result, the HR65 scaling overpredicts the residual estuarine circulation during neap tidal conditions when the advective contributions are minimal and underpredicts the residual estuarine circulation during spring tidal conditions when the advective contribution is maximal. In contrast, the Ri_x scaling neglects both the advective momentum flux and the interfacial turbulent stress. However, these two processes have a roughly equal and opposite effect on the residual estuarine circulation throughout the spring–neap cycle and over an order of magnitude change in river discharge, as seen by the roughly linear relationship in Fig. 9. Paradoxically, the scaling that is a more complete representation of the physics (HR65) demonstrates lower skill. It must be emphasized that the predictive skill of the Ri_x scaling in the Hudson River is misleading because it does not accurately represent the physics that govern the residual circulation.

In applying the HR65 and Ri_x scalings, C_o and A_o were treated as constant empirical parameters for each location in the estuary. The subtidal variation of these parameters can be examined by rearranging Eqs. (4) and (5) and solving for C_o and A_o, respectively. Because the scaling of the residual estuarine circulation has an inverse dependence on these coefficients, a decrease in their value suggests that there are processes adding to the residual estuarine circulation that are not accounted for in the scaling. In Fig. 10a, the spring–neap variations in the value of C_o are plotted against the advective momentum flux into the lower layer. For each model run, the contribution of the advective mo-

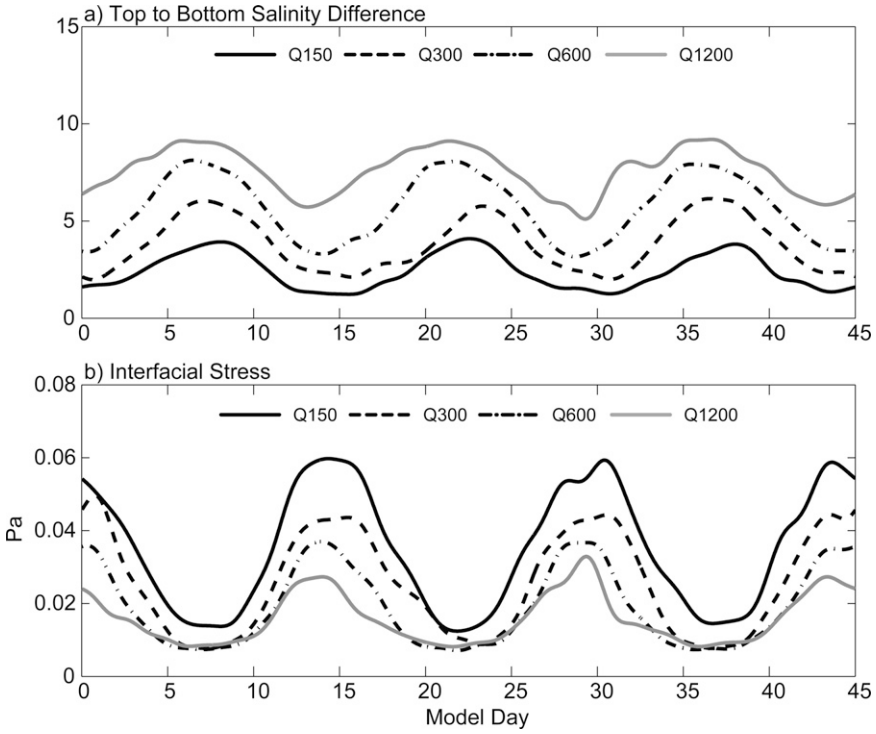

FIG. 8. (a) Salinity difference and (b) turbulent momentum flux (interfacial stress) between the residual inflowing bottom layer and outflowing surface layer. Values have been low-pass filtered (35 h) to remove tidal variability and averaged over the entire estuarine portion of the domain (averaged salinity <5 psu). Values from all simulated river discharges are shown: 150 $m^3\ s^{-1}$ (solid black line), 300 $m^3\ s^{-1}$ (dashed black line), 600 $m^3\ s^{-1}$ (dashed–dotted–dashed line), and 1200 $m^3\ s^{-1}$ (solid gray line).

mentum flux and the value of C_o are averaged spatially over the estuarine portion of the domain but allowed to vary through the spring–neap cycle. There is a strong spring–neap modulation of the value of C_o that is inversely correlated with the strength of the advective terms. The roughly linear relationship between these two quantities suggests that most of the error associated with the HR65 scaling is due to the omission of the advective terms. The influence of the interfacial stress largely is accounted for through the eddy coefficient, which exhibits a roughly linear relationship with the interfacial stress (Table 1). In contrast, the value of A_o is relatively constant over a wide range of tidal and river forcing (Fig. 10b and Table 2). This behavior is consistent with the greater skill exhibited using this scaling.

c. Tidal asymmetries in turbulent mixing

Figure 8 demonstrates that subtidal changes in stratification play an important role in reducing turbulent mixing and modifying the residual estuarine circulation. Jay and Musiak (1994) suggested that asymmetries in vertical mixing between flood and ebb tides caused by tidal straining of the along-channel density gradient could play an important role in generating residual circulation in estuaries. They argued that tidal straining of the along-channel density gradient reduces the turbulent mixing during ebb relative to flood tide. As a result, the vertical shear is enhanced during ebb as compared to flood, which combines to result in a two-layer tidally averaged residual circulation qualitatively similar to a baroclinically driven flow. The impact of the advective momentum terms described in this paper has similarities to the internal asymmetry described by Jay and Musiak (1994). However, in this study the asymmetry arises from advective momentum fluxes and not turbulent momentum fluxes. The stronger lateral flows observed during flood tide are more effective at redistributing momentum than during ebb when the lateral flows are suppressed. This reduces the shear during flood relative to ebb, effectively increasing the tidally averaged residual circulation. This is shown in Fig. 4, where the advective momentum flux clearly enhances the subtidal shear. In contrast, the turbulent momentum flux acts to reduce the shear between the inflowing and outflowing layers. The magnitude of the turbulent

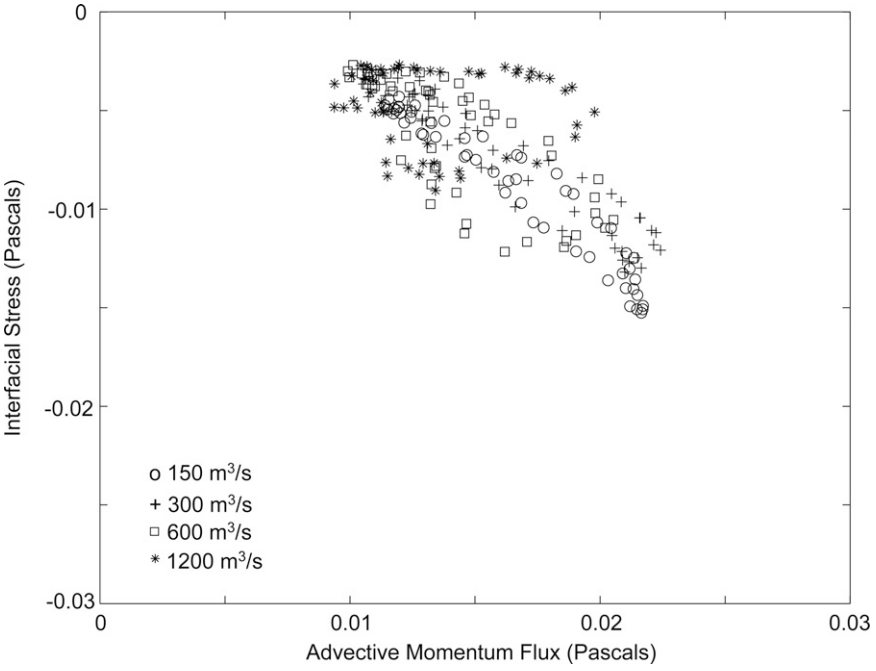

FIG. 9. Comparison of the advective and turbulent momentum flux into the lower layer for all modeled river discharges, circles: 150 $m^3 s^{-1}$, crosses: 300 $m^3 s^{-1}$, squares: 600 $m^3 s^{-1}$, and stars: 1200 $m^3 s^{-1}$. Both terms were spatially averaged over the entire estuarine extent of the model domain but allowed to vary subtidally in time as a function of tidal energy.

momentum flux between inflowing and outflowing layers is larger during ebb than flood, opposite of the pattern expected due to tidal straining. This occurs because the tidal patterns of stratification are significantly complicated by lateral flows, and the expected pattern of greater stratification during ebb tide is not observed over large portions of the estuarine cross section, as discussed by Scully and Friedrichs (2007). As a result, the asymmetries in mixing observed in this study are opposite of the pattern proposed by Jay and Musiak and act to reduce the residual circulation.

d. Tidal rectification by Ekman dynamics

The contribution of the advective momentum flux terms to the residual estuarine circulation described in

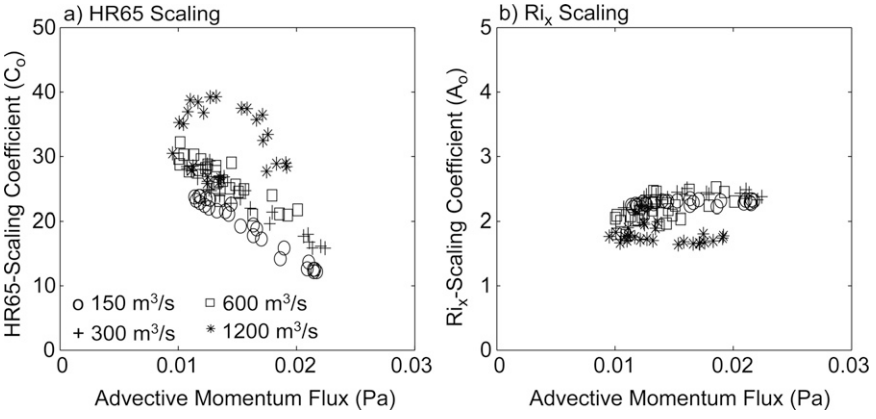

FIG. 10. Comparison of the behavior of the model coefficients for the (a) HR65 scaling and (b) Ri_x scaling compared to the advective momentum flux into the lower layer for all modeled river discharges, circles: 150 $m^3 s^{-1}$, crosses: 300 $m^3 s^{-1}$, squares: 600 $m^3 s^{-1}$, and stars: 1200 $m^3 s^{-1}$. All terms were spatially averaged over the entire estuarine extent of the model domain but allowed to vary subtidally in time as a function of tidal energy.

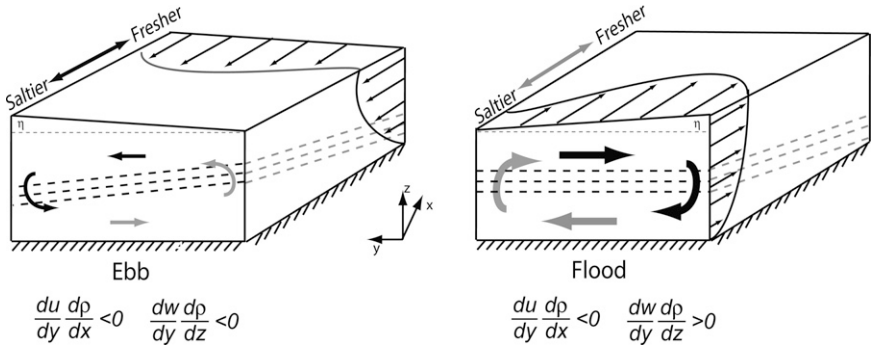

FIG. 11. Conceptual model for nonlinear tidal rectification by lateral Ekman transport in a simple tidal channel. During ebb the lateral advective terms induce a lateral shear in the along-channel flow that results in a lateral baroclinic pressure gradient that *reinforces* the lateral baroclinic pressure gradient driven by Ekman transport, enhancing the Ekman shutdown ($\partial u/\partial y\ \partial\rho/\partial x < 0$ and $\partial w/\partial y\ \partial\rho/\partial z < 0$). During flood the lateral advective terms induce a lateral shear in the along-channel flow that results in a lateral baroclinic pressure gradient that *opposes* the lateral baroclinic pressure gradient driven by Ekman transport, preventing the Ekman shut down ($\partial u/\partial y\ \partial\rho/\partial x < 0$ and $\partial w/\partial y\ \partial\rho/\partial z > 0$). The resulting tidal asymmetry in the strength of the lateral flow, combined with the sense of lateral shear caused by the advective terms, enhance both the vertical and lateral shear in the subtidal residual estuarine circulation, favoring inflow near the bed and on the right-hand side (when looking upestuary) of the channel.

section 3 can be thought of as tidal rectification of the lateral Ekman dynamics. This rectification mechanism was recently highlighted by Huijts et al. (2008), who derive the contribution of the lateral advective terms analytically. Their results are largely consistent with those presented here. One of the key aspects of this rectification mechanism is the asymmetry in the strength in the lateral flow. In both the modeling simulations presented here, as well as estuarine observations, the lateral flow is observed to be stronger during flooding tides. While the tidal asymmetry in the strength of the lateral circulation contributes to the importance of the lateral advective terms, a feedback exists where lateral advection enhances the tidal asymmetry in the lateral flow. This is conceptually illustrated in Fig. 11 for an idealized estuarine channel of uniform depth.

During ebb tide, the lateral Ekman transport in the bottom boundary layer is to the left of the flow with a compensatory flow in the surface layer in the opposite direction. This has two important consequences for the lateral baroclinic pressure gradient. First, this pattern of lateral circulation distorts the isopycnal surfaces, inducing a baroclinic pressure gradient that opposes the Ekman transport in the bottom boundary layer ($\partial w/\partial y\ \partial\rho/\partial z < 0$). Secondly, high momentum surface water is advected down into the boundary layer on the left-hand side of the channel, while slow low-momentum boundary layer water is upwelled along the right-hand side. This effectively induces a lateral shear in the along-channel flow. The interaction between the lateral shear in the along-channel flow and the along-channel density gradient induces a lateral baroclinic pressure gradient that reinforces the lateral baroclinicity caused by the Ekman transport ($\partial u/\partial y\ \partial\rho/\partial x < 0$). Thus, there is a negative feedback that hastens the Ekman shutdown during ebb. The opposite is true during flood when the lateral Ekman transport in the bottom boundary layer is toward the left side of the channel. In the absence of other processes, this Ekman transport would induce a lateral baroclinic pressure gradient that would effectively balance the Ekman forcing ($\partial w/\partial y\ \partial\rho/\partial z > 0$). In contrast to ebb, however, the lateral shear in the along-channel flow (induced by the lateral advective terms) interacts with the along-channel density gradient causing a lateral baroclinic pressure gradient that opposes the lateral baroclinicity caused by the Ekman transport ($\partial u/\partial y\ \partial\rho/\partial x < 0$). A positive feedback results that prevents the Ekman shutdown from occurring and allows relatively strong lateral flows to persist during flood.

This rectification process impacts both vertical and lateral shear of the residual estuarine circulation. As described by Lerczak and Geyer (2004), the tidal asymmetry in the strength of the lateral flow preferentially reduces the vertical shear on flood, which enhances the tidally averaged vertical shear in the residual estuarine circulation. Additionally, the lateral Ekman transport on both flood and ebb induce a lateral shear in the along-channel flow through the advective terms that has the same sign. This preferentially favors inflow on

the right-hand side and outflow on the left-hand side (when looking upestuary in the Northern Hemisphere). In reality, variable lateral bathymetry complicates this conceptual model somewhat, but it is important to note that this process would be expected even for systems with uniform lateral bathymetry. Differential advection caused by the frictional effects of lateral bathymetry seen in well-mixed estuaries (e.g., Nunes and Simpson 1985) is not necessary to create the tidal asymmetry in the strength of the lateral circulation.

e. Implication for other estuaries

Both the overall importance of the advective terms to the subtidal momentum balance and the compensatory relationship between the advective and turbulent stresses illustrated in this study raise the question of the generality of these results to other systems. The more idealized results of both Lerczak and Geyer (2004) and Huijts et al. (2008) suggest that advective processes play a leading order role in controlling the residual estuarine circulation. More generally, we would expect the importance of advection to decrease with increasing aspect ratio (width/depth) as both lateral and vertical shear are expected to decrease with increased aspect ratio. As discussed above, the flux of momentum between the upper and lower layers is most effective when the lateral circulation exhibits a distinct two-layer structure. This is often the case in relatively shallow estuarine systems. However, as shown in section 3c, the vertical structure of the lateral circulation can transition to a three-layer structure under strong stratification. Generally, this transition should occur when the bottom Ekman layer thickness becomes smaller than half the water depth. This suggests that the rectification of secondary flows should be less important in highly stratified and/or deep estuaries.

It is unclear if the compensatory relationship between the advective momentum flux and the interfacial friction is unique to the Hudson River: analysis of other estuarine systems is needed. The strong spring–neap modulation of both turbulent mixing and the vertical structure of the lateral flow exhibited in the Hudson River is also documented in other partially mixed estuaries such as the York River (Scully 2005). In these systems, where the along-channel bathymetry is relatively uniform, the relationship between the spring–neap variations in turbulent mixing and the advective terms is expected to be similar to the results from the Hudson. Similar results would not be expected for systems with more complex bathymetry. The MacCready (2007) model, which is based on the Ri_x scaling, agreed well with observations from the Hudson River, but did not agree favorably with the strongly funnel-shaped Delaware Bay. Detailed examination of the dynamics of the residual flow in other systems such as the Delaware is warranted. The skill of the Ri_x scaling in the Hudson should not be misinterpreted: our results suggest it is getting the right answer for the wrong reason.

5. Summary and conclusions

In this paper, utilizing realistic numerical simulations of the Hudson River estuary, we have demonstrated that tidal rectification of lateral advection acts as a driving force for the residual estuarine circulation. The nonlinear lateral advective terms contribute to the subtidal along-channel momentum balance at leading order. For spring tides during low flow conditions, the momentum flux on the lower layer by lateral advection approaches the pressure gradient forcing. The dynamics driving the lateral flow are consistent with Ekman transport in the bottom boundary layer. Lateral flows during flooding tide are stronger than observed during the ebb. The tidal asymmetry in lateral flow preferentially reduces the vertical shear on flood, which enhances the tidally averaged vertical shear in the residual estuarine circulation. Additionally, the lateral Ekman transport on both flood and ebb induce a lateral shear in the along-channel flow through the advective terms that have the same sign. This preferentially favors inflow on the right-hand side and outflow on the left-hand side (when looking upestuary in the Northern Hemisphere). The advective momentum flux acting on the lower layer has a strong spring–neap modulation, which is largely driven by the spatial correlation between the advective terms and the subtidal baroclinic forcing. The presence of density stratification significantly damps turbulent motions, reducing the interfacial stress between the inflowing and outflowing layers. As a result, the interfacial stress has a strong dependence on both the spring–neap cycle as well as the river discharge. Despite the importance of the nonlinear advective terms in driving the residual estuarine circulation, a linear scaling based on the horizontal Richardson number shows predictive skill for all of the model runs conducted. It should be noted that this skill is largely fortuitous, as it does not take into account two leading-order processes: nonlinear advection and interfacial friction. The apparent success of this scaling is due to the fact that these two processes, both of which are strongly influenced by the presence of density stratification, largely have a compensatory impact on the residual estuarine circulation in the Hudson River.

Acknowledgments. The authors are indebted to John Warner for his assistance in implementing the ROMS

simulations of the Hudson River. This manuscript benefited from the thoughtful comments of two anonymous reviewers. This research was supported by the Beacon Institute for Rivers and Estuaries—Woods Hole Oceanographic Institution postdoctoral fellowship program, as well as NSF Grants OCE-0452054 and OCE-0451740.

REFERENCES

Chatwin, P. C., 1976: Some remarks on the maintenance of the salinity distribution in estuaries. *Estuarine Coastal Mar. Sci.,* **4,** 555–566.

Geyer, W. R., J. H. Trowbridge, and M. M. Bowen, 2000: The dynamics of a partially mixed estuary. *J. Phys. Oceanogr.,* **30,** 2035–2048.

Godfrey, J. S., 1980: A numerical model of the James River estuary, Virginia, U.S.A. *Estuarine Coastal Mar. Sci.,* **11,** 295–310.

Hansen, D. V., and M. Rattray, 1965: Gravitational circulation in straits and estuaries. *J. Mar. Res.,* **23,** 104–122.

Huijts, K. M. H., H. M. Schuttelaars, H. E. de Swart, and C. T. Friedrichs, 2008: Analytical study of the transverse distribution of along-channel and transverse residual flows in tidal estuaries. *Cont. Shelf Res.,* in press.

Jay, D. A., and J. D. Musiak, 1994: Internal tidal asymmetry in channel flows: Origins and consequences. *Mixing in Estuaries and Coastal Seas*, C. Pattiaratchi, Ed., Vol. 50, *Coastal and Estuarine Studies*, Amer. Geophys. Union, 211–249.

Kantha, L. H., and C. A. Clayson, 1994: An improved mixed layer model for geophysical application. *J. Geophys. Res.,* **99,** 25 235–25 266.

Lerczak, J. A., and W. R. Geyer, 2004: Modeling the lateral circulation in straight, stratified estuaries. *J. Phys. Oceanogr.,* **34,** 1410–1428.

——, ——, and R. J. Chant, 2006: Mechanisms driving the time-dependent salt flux in a partially stratified estuary. *J. Phys. Oceanogr.,* **36,** 2296–2311.

MacCready, P., 2007: Estuarine adjustment. *J. Phys. Oceanogr.,* **37,** 2133–2145.

Monismith, S. G., W. Kimmerer, J. R. Burau, and M. T. Stacey, 2002: Structure and flow-induced variability of the subtidal salinity field in northern San Francisco Bay. *J. Phys. Oceanogr.,* **32,** 3003–3019.

Nunes, R. A., and J. H. Simpson, 1985: Axial convergence in a well-mixed estuary. *Estuarine Coastal Shelf Sci.,* **20,** 637–649.

Pritchard, D. W., 1952: Estuarine hydrography. *Advances in Geophysics,* Vol. 1, Academic Press, 243–280.

——, 1954: A study of the salt balance in a coastal plain estuary. *J. Mar. Res.,* **13,** 133–144.

——, 1956: The dynamic structure of a coastal plain estuary. *J. Mar. Res.,* **15,** 33–42.

Ralston, D. K., W. R. Geyer, and J. A. Lerczak, 2008: Subtidal salinity and velocity in the Hudson River estuary: Observations and modeling. *J. Phys. Oceanogr.,* **38,** 753–770.

Scully, M. E., 2005. The interaction between stratification, circulation, and sediment transport in a partially mixed estuary. Ph.D. dissertation, School of Marine Science, College of William and Mary, 148 pp.

——, and C. T. Friedrichs, 2003: The influence of asymmetries in overlying stratification on near bed turbulence and sediment suspension in a partially mixed estuary. *Ocean Dyn.,* **53,** 208–219.

——, and ——, 2007: The importance of tidal and lateral asymmetries in stratification to residual circulation in partially mixed estuaries. *J. Phys. Oceanogr.,* **37,** 1496–1511.

——, ——, and J. M. Brubaker, 2005: Control of estuarine stratification and mixing by wind-induced straining of the estuarine density field. *Estuaries,* **28,** 321–326.

Stacey, M. T., S. G. Monismith, and J. R. Burau, 1999: Observations of turbulence in a partially stratified estuary. *J. Phys. Oceanogr.,* **29,** 1950–1970.

——, J. R. Burau, and S. G. Monismith, 2001: Creation of residual flows in a partially stratified estuary. *J. Geophys. Res.,* **106,** 17 013–17 037.

Trowbridge, J. H., W. R. Geyer, M. M. Bowen, and A. J. Williams, 1999: Near-bottom turbulence measurements in a partially mixed estuary: Turbulent energy balance, velocity structure, and along-channel momentum balance. *J. Phys. Oceanogr.,* **29,** 3056–3072.

Uncles, R. J., and J. A. Stephens, 1990: The structure of vertical current profiles in a macrotidal, partially-mixed estuary. *Estuaries,* **13,** 349–361.

Warner, J. C., W. R. Geyer, and J. A. Lerczak, 2005: Numerical modeling of an estuary: A comprehensive skill assessment. *J. Geophys. Res.,* **110,** C05001, doi:10.1029/2004JC002691.

Wilmott, C. J., 1981: On the validation of models. *Phys. Geogr.,* **2,** 184–194.